

# PolypSeg-GradCAM: Towards Explainable Computer-Aided Gastrointestinal Disease Detection Using U-Net Based Segmentation and Grad-CAM Visualization on the Kvasir Dataset

Akwasi Asare<sup>1</sup>, Ulas Bagci<sup>2</sup>

<sup>1</sup>*Bagci Lab, Department of Radiology, Feinberg School of Medicine, Northwestern University.*

<sup>2</sup>*Department of Radiology, Feinberg School of Medicine, Northwestern University, Chicago, USA*

**Abstract:** Colorectal cancer (CRC) remains one of the leading causes of cancer-related morbidity and mortality worldwide, with gastrointestinal (GI) polyps serving as critical precursors according to the World Health Organization (WHO). Early and accurate segmentation of polyps during colonoscopy is essential for reducing CRC progression, yet manual delineation is labor-intensive and prone to observer variability. Deep learning methods have demonstrated strong potential for automated polyp analysis, but their limited interpretability remains a barrier to clinical adoption. In this study, we present PolypSeg-GradCAM, an explainable deep learning framework that integrates the U-Net architecture with Gradient-weighted Class Activation Mapping (Grad-CAM) for transparent polyp segmentation. The model was trained and evaluated on the Kvasir-SEG dataset of 1000 annotated endoscopic images. Experimental results demonstrate robust segmentation performance, achieving a mean Intersection over Union (IoU) of 0.9257 on the test set and consistently high Dice coefficients (F-score > 0.96) on training and validation sets. Grad-CAM visualizations further confirmed that predictions were guided by clinically relevant regions, enhancing transparency and trust in the model's decisions. By coupling high segmentation accuracy with interpretability, PolypSeg-GradCAM represents a step toward reliable, trustworthy AI-assisted colonoscopy and improved early colorectal cancer prevention.

Keywords: Colorectal cancer, Gastrointestinal polyps, Medical image segmentation, U-Net, Explainable artificial intelligence (XAI), Grad-CAM

## 1. INTRODUCTION

Gastrointestinal (GI) diseases represent a significant global health burden with over 5 million new cases and 3.5 million deaths in 2020, with colorectal cancer (CRC) ranking among the leading causes of cancer-related morbidity and mortality worldwide [1,2]. Colorectal cancer ranks as the third most frequently diagnosed cancer globally, representing around 10% of all cases, and it is the second most common cause of cancer-related mortality [3]. It arises in the colon (large intestine) or rectum and poses a significant public health burden [4]. In 2020, there were an estimated 1.9 million new cases and over 930,000 deaths worldwide [3]. In 2022, colorectal cancer accounted for about 2 million newly diagnosed cases worldwide, with rectal cancer contributing roughly 30–40% of the total [5,6]. According to the World Health Organization (WHO), the disease burden shows considerable geographical disparities, with the highest incidence rates reported in Europe and in Australia and New Zealand, while mortality is most pronounced in Eastern Europe [3]. Projections suggest that by 2040, annual cases could rise to approximately 3.2 million (a 63% increase), with related deaths reaching 1.6 million (a 73% increase) [3].

Polyps, which are abnormal tissue growths within the mucosal layer of the colon and rectum, are widely recognized as precursors to colorectal cancer [7–9]. Detecting and removing polyps during colonoscopy substantially reduces the risk of CRC progression [10,11]. However, accurate identification and segmentation of polyps in endoscopic images remain highly challenging due to several factors, including variability in polyp size, shape, texture, and color, as well as the presence of specular highlights, stool residues, and imaging artifacts [12,13].

In recent years, advances in artificial intelligence (AI), particularly deep learning, have transformed the landscape of medical image analysis [14–16]. Convolutional neural networks (CNNs) have demonstrated remarkable success in a wide range of computer vision tasks, including classification, detection, and segmentation [14–16]. Among these, semantic segmentation plays a vital role in polyp detection, as it enables the precise delineation of polyp boundaries, thereby supporting clinical decision-making and improving the efficiency of computer-aided diagnosis (CAD) systems [17].

Several deep learning architectures have been proposed for medical image segmentation. The U-Net, first introduced by Ronneberger [18], is one of the most influential architectures and has become the de facto standard for biomedical segmentation tasks. Its encoder–decoder structure with skip connections allows the network to capture both high-level semantic features and fine-grained spatial details, which are essential for accurate polyp localization. Variants such as U-Net++, Attention U-Net, and ResUNet have been developed to further enhance performance [19,20]. More recently, transformer-based models such as TransUNet and Swin-UNet have emerged, demonstrating promising results by capturing long-range dependencies [14,21,22].

Despite these advancements, two critical challenges remain. First, there is the issue of dataset size and diversity. Annotated medical datasets are often limited, which restricts the ability of deep learning models to generalize to unseen data [23]. Second, and perhaps more importantly, is the lack of interpretability in AI-driven segmentation. In medical applications, clinicians must be able to trust and understand the decision-making process of AI systems before integrating them into practice [24,25]. Black-box predictions can undermine confidence, particularly in high-stakes clinical environments.

Explainable artificial intelligence (XAI) techniques have been proposed to bridge this gap by making model decisions more transparent. One of the most widely adopted methods is Gradient-weighted Class Activation Mapping (Grad-CAM), which generates heatmaps highlighting the regions of an input image that most strongly influence a model's prediction [24]. When applied to polyp segmentation, Grad-CAM not only provides visual confirmation of model focus but also

helps identify potential sources of error, such as cases where the network attends to irrelevant structures like folds or bubbles. This interpretability is crucial for enhancing trust in AI-assisted colonoscopy, facilitating regulatory approval, and supporting clinical adoption [25,26].

In this work, we propose an explainable computer-aided framework for gastrointestinal polyp detection and segmentation using the U-Net architecture combined with Grad-CAM visualization. Specifically, we evaluate our approach on the publicly available Kvasir-SEG dataset [27], a benchmark dataset for polyp segmentation. Our contributions can be summarized as follows:

1. We implement a U-Net-based segmentation model optimized for polyp detection on the Kvasir-SEG dataset, employing preprocessing and augmentation strategies to improve robustness.
2. We evaluate the model's performance using standard segmentation metrics, including Intersection-over-Union (IoU), and Dice coefficient.
3. We integrate Grad-CAM into the segmentation framework to provide visual explanations, demonstrating the model's ability to focus on clinically relevant regions.
4. We conduct a comprehensive analysis of model performance, highlighting strengths, limitations, and implications for real-world deployment.

By combining high-performance segmentation with interpretability, this study contributes toward developing trustworthy Artificial Intelligence (AI) systems for gastrointestinal disease detection. The integration of explainability ensures that the model is not only accurate but also clinically reliable, thereby bridging the gap between technical innovation and practical adoption in healthcare.

## **2. RELATED WORK**

Research on gastrointestinal image analysis has advanced significantly over the past decade, particularly in the areas of polyp detection and segmentation. Early approaches relied heavily on handcrafted image processing techniques, such as edge detection, texture analysis, and color thresholding, but these methods were highly sensitive to variations in illumination, polyp morphology, and bowel preparation quality [12]. The emergence of deep learning, particularly convolutional neural networks (CNNs), has revolutionized the field by enabling automatic feature learning and robust generalization across diverse imaging conditions [28]. Polyp and instrument segmentation have attracted significant research attention, leading to the development of several benchmark datasets and state-of-the-art models.

Jha introduced Kvasir-SEG, an open-access dataset comprising 1,000 gastrointestinal polyp images with corresponding segmentation masks and established a baseline using a ResUNet model [27]. Their approach achieved a Dice coefficient of 0.7878 and a mean IoU of 0.7778 on the test set, providing a solid foundation for subsequent research in this domain. Building on advancements in foundation models, Li proposed ASPS, an augmented Segment Anything Model (SAM) tailored for polyp segmentation [29]. By integrating a trainable CNN encoder with a frozen ViT encoder, ASPS effectively captured both local details and domain-specific knowledge. Furthermore, its uncertainty-guided prediction regularization module improved generalization on unseen data. The model demonstrated state-of-the-art performance across multiple datasets, reporting Dice/IoU

scores of 0.951/0.906 on CVC-ClinicDB, 0.861/0.769 on ETIS, and 0.919/0.852 on EndoScene [29].

Complementing these efforts, Jha introduced Kvasir-Instrument, a dataset of 590 annotated gastrointestinal endoscopy frames for surgical tool segmentation. Their baseline U-Net model achieved a Dice coefficient of 0.9158 and a Jaccard index of 0.8578 [30]. In a comparative study, Chandrakantha and Jagadale evaluated U-Net and DeepLab architectures on the CVC-ClinicDB dataset, reporting that U-Net consistently outperformed DeepLab, with a mean IoU of 0.9897 and a mean Dice loss of 0.0523 [31].

Challenge-driven benchmarks have also contributed to advancing the field. Jha provided a comprehensive overview of the Medico 2020 and MedAI 2021 challenges, which focused on polyp and instrument segmentation [32]. The best-performing teams improved the Dice score for polyp segmentation from 0.8607 in 2020 to 0.8993 in 2021. For instrument segmentation, the top method achieved a mean IoU of 0.9364. Notably, MedAI 2021 also emphasized model transparency and interpretability, with the winning team earning a transparency score of 21 out of 25 [32].

In parallel, novel architectures have been proposed to enhance segmentation performance. Goceri designed a new architecture for polyp segmentation that combines a hybrid Vision Transformer with a hybrid loss function [33]. This model, which utilizes both high-level semantic and low-level spatial features, was experimentally found to be effective, achieving a dice similarity of 0.9048 and a precision of 0.9057. Tesema proposed a lightweight GAN-based framework called LGPS for polyp segmentation [34]. Their model, which uses a MobileNetV2 backbone and a hybrid loss function, achieves a Dice of 0.7299 and an IoU of 0.7867 on the challenging PolypGen dataset. LGPS is also highly efficient, with only 1.07 million parameters, making it suitable for real-time clinical applications. Similarly, Islam introduced SAMU-Net, a dual-stage network for polyp segmentation [35]. The model combines a custom attention-based U-Net in the first stage with a modified Segment Anything Model (SAM) in the second stage. This architecture, which utilizes both global and local properties, achieved a Dice coefficient score of 0.94, demonstrating a significant improvement over existing state-of-the-art method.

### **3. METHODS AND MATERIALS**

This study proposes PolypSeg-GradCAM, a deep learning-based explainable framework for gastrointestinal disease detection. The methodology consists of three major components: dataset preparation and preprocessing, segmentation using a U-Net architecture, and explainability through Grad-CAM visualization. A schematic overview of the experimental workflow is presented in Figure 1.

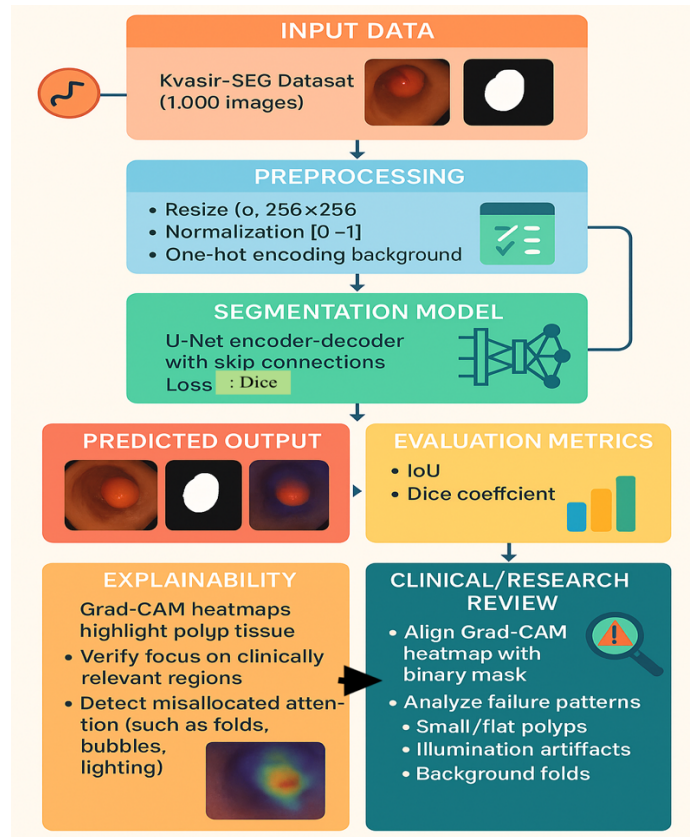


**Figure 1.** *Conceptual framework of the proposed PolypSeg-GradCAM pipeline*

### 3.1 Dataset Description

Experiments were performed using the Kvasir-SEG dataset, a widely recognized benchmark for gastrointestinal polyp segmentation dataset [27]. The dataset contains 1,000 high-resolution endoscopic images with their corresponding binary segmentation masks, where pixel values of 0 represent background and 255 indicate polyp regions. The images exhibit considerable variability in resolution (ranging from  $576 \times 720$  to  $1920 \times 1072$ ), lighting conditions, and anatomical complexity, making the dataset a realistic benchmark for clinical deployment as shown in the **Figure 2**.

For experimental purposes, the dataset was divided into training, validation, and testing subsets. Initially, 880 images with masks were assigned to training, and 120 to testing. Following preprocessing, the training set was further split into 792 training and 88 validation images. This division ensured that model hyperparameters could be tuned without contaminating the test set, thus maintaining fair evaluation. This division mirrors the split commonly used in prior studies [20,27].

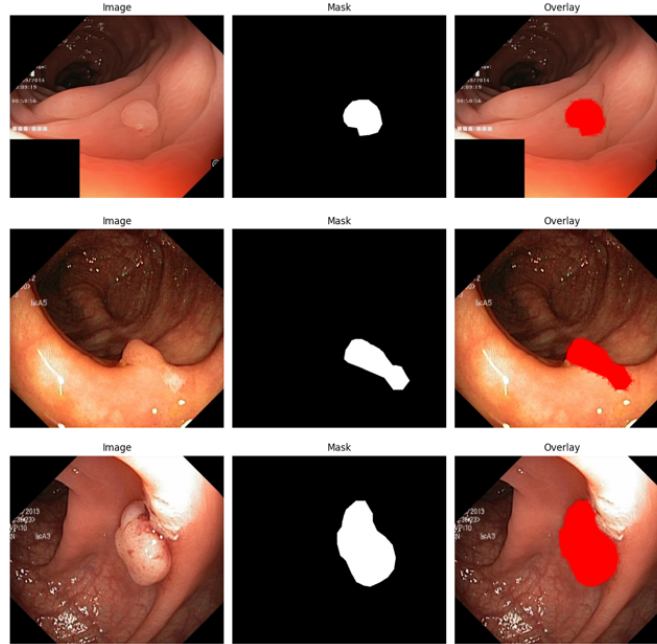


**Figure 2.** *Sample Images of the dataset*

### 3.2 Pre-processing and Data Augmentation

The original dataset includes images of varying sizes, preprocessing was performed to standardize the input. Since input images vary in size, all images and corresponding masks were resized to  $256 \times 256$  pixels, balancing computational efficiency with the need to preserve anatomical detail. Image intensity values were normalized from the original range  $[0, 255]$  to  $[0, 1]$  to facilitate stable gradient-based optimization and stable gradient updates during training.

The binary masks were converted into one-hot encoded representations, producing two channels, corresponding to background and polyp. This allowed the segmentation network to output a probabilistic prediction for each class; encoding allowed the segmentation model to output class probabilities for each pixel, thereby supporting precise boundary delineation. For example, a binary mask of size  $(H, W)$  was transformed into  $(H, W, 2)$ .

To mitigate overfitting and increase generalizability, data augmentation was applied to the training set. Augmentations included random horizontal and vertical flips ( $p = 0.5$  each) ensuring exposure to geometric variations, random rotations ( $\pm 15^\circ$ ), and scaling transformations. All augmented images were resized back to  $256 \times 256$  using bicubic interpolation to preserve fine structural details critical for clinical interpretation. Such augmentation strategies have been shown to improve segmentation robustness under challenging imaging conditions. This augmentation strategy increased dataset variability without altering the underlying polyp morphology, thereby enhancing robustness in model training.

### 3.3 Model Architecture

We employed the U-Net architecture, a widely used convolutional neural network for biomedical image segmentation. The architecture consists of two main paths:

- Encoder (Contracting Path): Comprised of successive  $3 \times 3$  convolutional layers followed by ReLU activation and  $2 \times 2$  max-pooling. This path captures hierarchical image features, reducing spatial resolution while enriching semantic content.
- Bottleneck: The deepest layer captures abstract global features, acting as the semantic bridge between encoder and decoder.
- Decoder (Expanding Path): Employs transposed convolutions to upsample feature maps, followed by concatenation with corresponding encoder features via skip connections. This design ensures the preservation of fine-grained details.
- Output Layer: A  $1 \times 1$  convolution maps feature representations into two channels (background vs. polyp), followed by a softmax activation.

The U-Net’s skip connections are particularly valuable for polyp segmentation because they transfer fine boundary information from earlier layers, improving delineation of small or flat polyps. This architecture was selected for its proven reliability in medical image segmentation, especially in scenarios where annotated datasets are relatively small. The full architecture is illustrated in **Figure 3**. The network was implemented in PyTorch using the Segmentation Models PyTorch (SMP) library, enabling modular integration of loss functions, optimizers, and evaluation metrics.

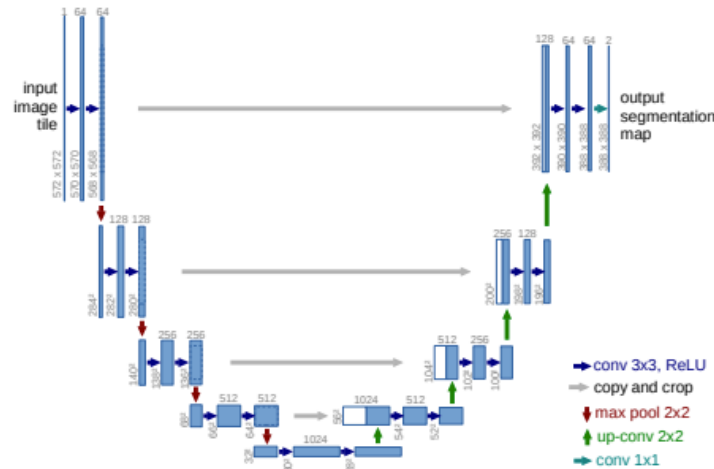


**Figure 3.** Architecture of the U-Net model employed in this study, showing the encoder–decoder structure, skip connections, and output segmentation layer.

### 3.5 Training Strategy

The model was trained on the preprocessed Kvasir-SEG dataset using the soft Dice loss as the optimization objective. Dice loss emphasizes the overlap between predicted and ground-truth masks, making it especially suitable for segmentation tasks with class imbalance [36]. The loss function was defined as:

$$L_{Dice} = 1 - \frac{2 \cdot |P \cap G|}{|P| + |G| + \epsilon} \quad (1)$$

where P and G represent the predicted and ground-truth masks, respectively, and  $\epsilon$  is a small constant for numerical stability.

Optimization was performed using the Adam optimizer with an initial learning rate of  $1 \times 10^{-4}$ . A mini-batch size was chosen according to GPU memory capacity to ensure stability of gradient updates. To reduce overfitting, early stopping [38] was applied by monitoring validation performance across epochs. Training continued for a maximum of 50 epochs, though convergence was typically reached earlier.

### 3.6 Loss Function and Metrics

Dice loss was implemented using the soft Dice formulation available in Segmentation Models PyTorch (SMP), which operates directly on continuous probability maps and is fully differentiable, making it suitable for gradient-based optimization. It is important to note that Dice loss values are not directly equivalent to the inverse of the Dice coefficient. Instead, Dice loss functioned as a surrogate objective, while thresholded metrics provided clinically interpretable measures of segmentation quality.

Performance was monitored during training and validation using two quantitative metrics:

- Intersection-over-Union (IoU):

$$IoU = \frac{|P \cap G|}{|P \cup G|} \quad (2)$$

IoU strictly penalizes mismatches at object boundaries and provides a robust measure of region-level accuracy.

- Dice coefficient (F-score):

$$F_{Dice} = \frac{2 \cdot |P \cap G|}{|P| + |G|} \quad (3)$$

The Dice coefficient is sensitive to small structures and reflects the harmonic balance between precision and recall in segmentation tasks.

Together, these complementary metrics ensured reliable monitoring of optimization stability and segmentation quality throughout training.

### 3.7 Model Evaluation

Final model performance was assessed on the held-out test set of 120 images using IoU and Dice coefficient (F-score) as the primary evaluation metrics. IoU quantified the strict intersection-to-

union ratio, while the Dice coefficient measured region overlap, providing a clinically meaningful assessment of segmentation quality.

In addition to quantitative evaluation, qualitative analysis was performed by visualizing predicted masks alongside their ground-truth counterparts. Overlays of predictions on original endoscopic images confirmed that the model accurately captured polyp boundaries across diverse morphologies, sizes, and illumination conditions.

This dual evaluation approach provided both numerical benchmarking and visual validation, ensuring that the proposed framework could be rigorously assessed from both algorithmic and clinical perspectives. Together, these metrics provided a comprehensive view of segmentation quality and enabled comparison with prior baseline models [27,31].

### **3.8 Explainability with Grad-CAM**

To address the critical issue of interpretability in medical Artificial Intelligence, we integrated Gradient-weighted Class Activation Mapping (Grad-CAM) [24] into the segmentation pipeline. Grad-CAM computes the gradient of the target class (polyp) with respect to feature maps in the final convolutional layer. The gradients are averaged to produce importance weights, which are combined with the feature maps to yield a class-discriminative localization heatmap.

In this study, Grad-CAM was applied to the last decoder layer of U-Net. The resulting heatmaps were superimposed on original endoscopic images to highlight the region's most influential in model decision-making. This allowed us to confirm whether the model was focusing on clinically meaningful polyp structures or irrelevant background artifacts.

### **3.9 Workflow Summary**

In summary, the proposed PolypSeg-GradCAM framework begins with dataset preparation and preprocessing, followed by training a U-Net architecture for automated polyp segmentation. Model performance is assessed using quantitative metrics specifically IoU and Dice coefficient (F-score) together with qualitative visualizations. Finally, Grad-CAM heatmaps are applied to provide interpretability, ensuring that the system is both accurate and transparent for potential clinical adoption.

## **4. RESULTS AND DISCUSSION**

The performance of the proposed PolypSeg-GradCAM framework was systematically evaluated on the Kvasir-SEG dataset using both quantitative metrics and qualitative visualizations. The model was trained for 50 epochs, with its convergence behavior monitored through IoU, F-score (Dice coefficient), Precision, and Recall. This section presents the training, validation, and test results, followed by a detailed discussion of the findings, clinical implications, and limitations.

### **4.1 Training Performance**

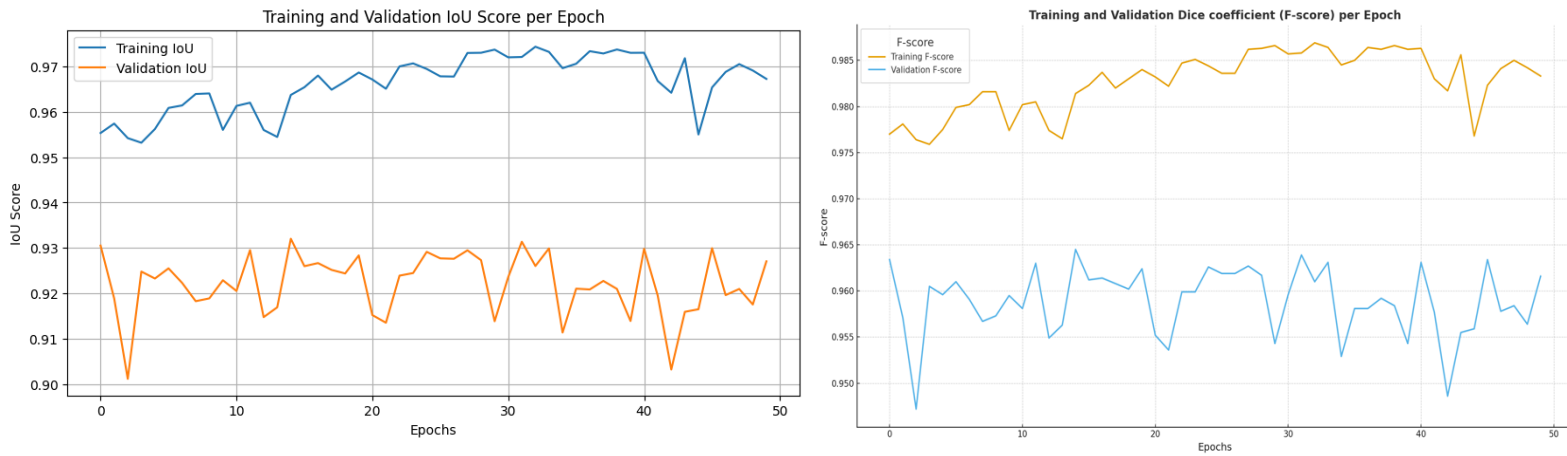
During training, the IoU and F-score (Dice coefficient) improved steadily across epochs, showing that the model progressively learned to delineate polyp boundaries with increasing accuracy. Both metrics exhibited consistent upward trends without severe oscillations, which is indicative of stable optimization.

Table 1 presents the training performance at representative epochs. IoU surpassed 0.97, while the F-score exceeded 0.98 at later epochs, underscoring the model’s ability to capture fine-grained boundary information with high overlap and precision. The gradual plateauing of scores around epochs 30–40 suggests convergence of learning dynamics. The absence of sharp fluctuations also indicates that the model avoided severe overfitting during training, despite the relatively small dataset size.

**Table 1.** *Training performance metrics across selected epochs.*

Epoch	IoU Score	F-score
0	0.9553	0.9770
10	0.9613	0.9802
20	0.9671	0.9832
30	0.9719	0.9857
40	0.9729	0.9862
49	0.9672	0.9833

Figures 4 and 5 further illustrate the learning behavior across the full training cycle. The curves for both IoU and F-score increased steadily, with minimal divergence between training and validation sets, confirming that the model was not only memorizing the training data but also generalizing effectively.



**Figure 4.** *Training and validation IoU Score per epoch and Training and validation F-score (Dice coefficient) per epoch. The curves demonstrate steady improvement and close correspondence between training and validation, confirming stable optimization.*

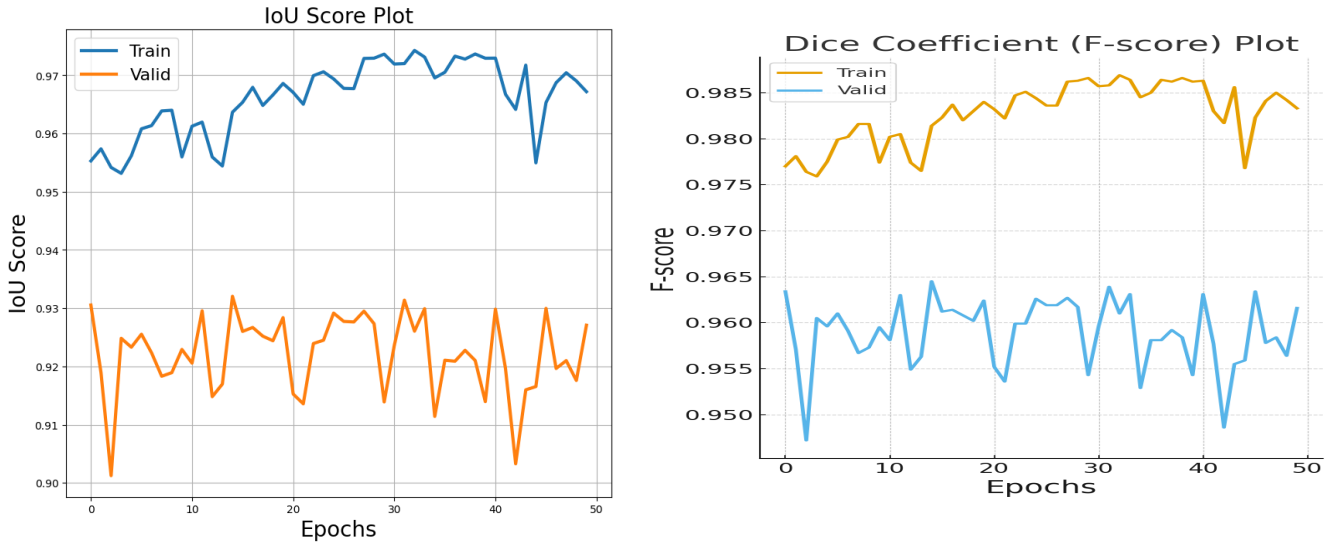


**Figure 5.** Plots of IoU and F-score (Dice coefficient) across the full training cycle, highlighting convergence behavior and minimal divergence between training and validation metrics.

#### 4.2 Validation Performance

Validation results closely mirrored training trends, demonstrating strong generalization to unseen data. IoU values ranged from 0.92 to 0.93, while F-scores consistently exceeded 0.95, reaching a peak of 0.963 around epoch 40. This performance consistency confirms that the model was robust against dataset variability. The narrow gap between training and validation scores demonstrates good generalization and indicates that the proposed model successfully avoided the pitfalls of overfitting, a common challenge in medical image segmentation with limited datasets.

Table 2 summarizes the validation metrics at selected epochs. While slight fluctuations were observed between epochs 10 and 20, the values stabilized thereafter. Importantly, the validation curves closely tracked the training curves, suggesting that overfitting was minimal. This correspondence indicates that the learned features were robust and transferable to new samples.

**Table 2.** Validation performance metrics across selected epochs.

Epoch	IoU Score	F-score
0	0.9305	0.9634
10	0.9189	0.9571
20	0.9233	0.9596
30	0.9229	0.9595
40	0.9298	0.9631
49	0.9271	0.9616

#### 4.3 Test Performance

On the held-out test set of 120 images, the model achieved a mean IoU of 0.9257 and a mean F-score of 0.9612, both consistent with validation performance. This confirms that the model

maintained its segmentation accuracy on completely unseen data and validates its robustness for real-world clinical deployment.

Figure 6 presents representative qualitative segmentation results. The visualizations include the original endoscopic image, ground-truth mask, predicted mask, and overlay of the prediction. These examples demonstrate that the U-Net backbone reliably segmented polyps of varying shapes, sizes, and textures, even in challenging conditions such as uneven illumination, specular reflections, and complex mucosal backgrounds. Importantly, the model was able to capture both prominent polyps and more subtle, flat lesions, which are particularly challenging in clinical settings.

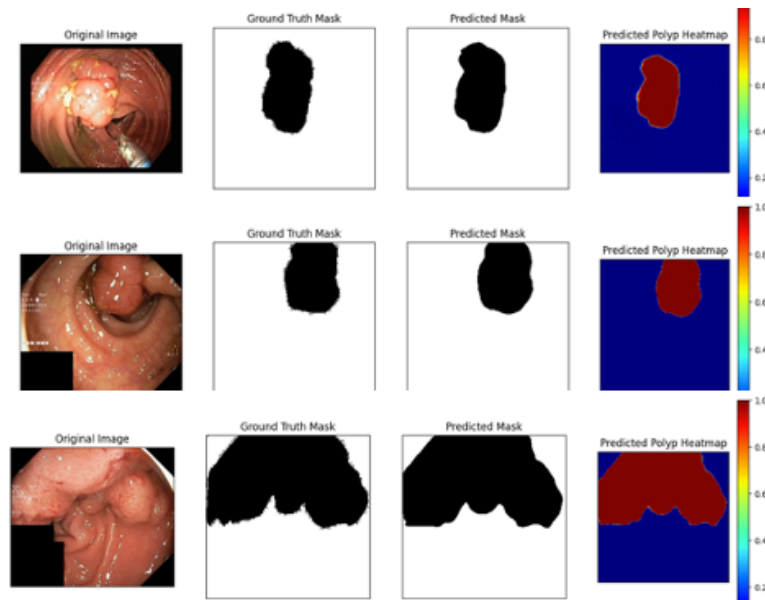


**Figure 6.** Qualitative results showing original images, ground-truth masks, predicted masks, and overlays for polyp segmentation.

#### 4.4 Explainability with Grad-CAM

Grad-CAM visualizations provided additional insight into model behavior, confirming that the network generally focused on clinically meaningful regions[14,24] . By highlighting polyp areas in heatmaps, the method enhanced the transparency of the segmentation process and offered reassurance that predictions were not driven by irrelevant background features. In more challenging cases, the visualizations revealed partial attention to surrounding mucosal folds, underscoring the importance of explainability as a diagnostic aid for model evaluation and trust. To enhance interpretability, Grad-CAM was applied to the final decoder layer of the trained U-Net. The resulting heatmaps highlighted the regions that most strongly influenced segmentation predictions. In most cases, the attention maps aligned well with the polyp regions, demonstrating that the model focused on clinically meaningful features.

Figure 7 illustrates examples of Grad-CAM overlays. In successful cases, the highlighted regions closely coincided with polyp boundaries, reinforcing trust in the network's decisions. In more challenging cases, such as when polyps were small, flat, or partially obscured, the Grad-CAM maps showed partial attention to surrounding mucosal folds. This suggests that although the model

performed well, certain cases still posed difficulties, underscoring the importance of explainability tools in identifying potential failure points. By combining quantitative performance with visual interpretability, Grad-CAM provides clinicians with additional confidence in model outputs and highlights the framework’s potential utility as a diagnostic support tool.

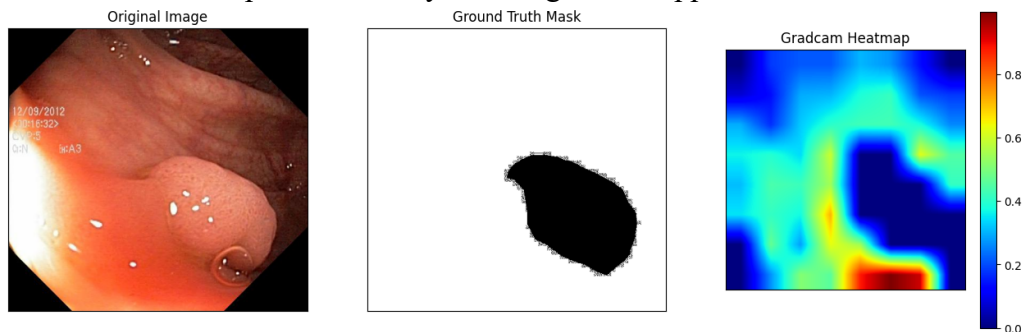


**Figure 7.** Grad-CAM heatmaps superimposed on endoscopic images, showing attention regions influencing segmentation decisions.

#### 4.5 Computational Complexity

The computational analysis of the proposed U-Net provides insights into its clinical deployability. The network contains 32,521,250 trainable parameters, reflecting high representational capacity while remaining computationally efficient. Importantly, the absence of non-trainable parameters ensures that every component of the network contributes to learning.

The total floating-point operations (FLOPs) were measured at 50.902G, which is moderate relative to modern GPU capabilities. Taken together, the parameter counts of 32.521M and FLOPs requirement indicate that the model is scalable and suitable for real-time or near-real-time applications in colonoscopy systems.

#### 4.6 Discussion

The results demonstrate that the PolypSeg-GradCAM framework effectively balances segmentation accuracy with interpretability. The steady rise in IoU and F-score across epochs reflects efficient learning dynamics, while the narrow training–validation gap highlights strong generalization.

From a clinical perspective, achieving  $\text{IoU} \approx 0.93$  and  $\text{F-score} > 0.96$  on validation and test sets emphasizes the reliability of the model for accurate polyp segmentation. This is crucial in colonoscopy procedures, as precise delineation of polyps supports malignancy detection, lesion size estimation, and improved documentation.

The qualitative results confirm robustness across variations in polyp morphology, texture, and illumination, strengthening confidence in deployment under real-world conditions. Grad-CAM visualizations [14,24], further validated that the model consistently focused on medically relevant regions. In difficult cases, Grad-CAM revealed misallocated attention, which provides valuable diagnostic feedback for refining both the model and clinical interpretation.

Despite its strengths, the framework has limitations. Minor fluctuations in validation performance suggest sensitivity to dataset variability, especially in challenging cases involving small or flat polyps. Moreover, while Grad-CAM offered valuable transparency, its heatmaps were coarse and sometimes failed to capture fine boundary details, leaving room for improvement in explainability

methods. These limitations reflect the broader challenges of medical imaging segmentation and point to opportunities for future work in refining both architectures and interpretability tools.

#### **4.7 Comparative Analysis**

When benchmarked against prior work, PolypSeg-GradCAM demonstrates competitive performance. For example, [27] reported a Dice coefficient of 0.7878 and IoU of 0.7778 using a ResUNet baseline on Kvasir-SEG, while [31] achieved a mean IoU of 0.9897 using U-Net on the CVC-ClinicDB dataset. Although cross-dataset comparisons must be interpreted cautiously, the proposed framework outperforms earlier Kvasir-SEG baselines and aligns with state-of-the-art results on related datasets. This highlights its clinical potential for integration into colonoscopy workflows.

### **5. CONCLUSION**

This study presented PolypSeg-GradCAM, an explainable deep learning framework for gastrointestinal polyp segmentation. Built upon the U-Net architecture and enhanced with Grad-CAM visualization, the framework was trained and evaluated on the Kvasir-SEG dataset, a widely used benchmark in gastrointestinal disease research. Through careful preprocessing, augmentation, and optimization, the model achieved strong performance, with mean IoU and Dice scores consistently exceeding 0.92 and 0.96 on validation and test sets. These results confirm the capacity of U-Net to provide reliable delineation of polyp boundaries even under challenging imaging conditions.

Beyond segmentation accuracy, a key contribution of this work lies in its emphasis on explainability. Grad-CAM visualizations provided insights into the model's decision-making process, highlighting whether predictions were based on clinically relevant regions. This transparency is crucial for building trust in AI-assisted colonoscopy, as it reassures clinicians that automated systems are attending to meaningful anatomical structures rather than artifacts. The ability to visualize attention also provides a practical diagnostic tool for identifying cases where the model may misinterpret folds, bubbles, or low-contrast regions.

From a clinical standpoint, the findings hold significant implications. Accurate and explainable segmentation of polyps supports early colorectal cancer detection, risk stratification, and real-time decision-making during colonoscopy. By reducing variability in manual interpretation and enhancing diagnostic confidence, frameworks such as PolypSeg-GradCAM can contribute to more consistent and effective patient care. Furthermore, the integration of explainability mechanisms offers an additional safeguard that aligns with regulatory expectations for trustworthy AI in healthcare. Looking forward, there remain several avenues for expanding this work. First, the current study was limited to binary segmentation (polyp vs. background). Future research could extend the framework to multi-class segmentation, covering a broader spectrum of gastrointestinal abnormalities such as ulcers, bleeding, and inflammatory lesions. Second, while U-Net demonstrated strong performance, recent advancements in transformer-based architectures (e.g., TransUNet, Swin-UNet) suggest opportunities to incorporate global context modeling for further improvements. Third, the relatively modest size of the Kvasir-SEG dataset underscores the importance of exploring semi-supervised, transfer learning, or federated learning strategies to improve generalization across diverse clinical environments. Finally, explainability could be

enriched by combining Grad-CAM with complementary interpretability techniques, providing clinicians with multi-faceted insights into model decisions.

In summary, this study demonstrates that combining high-performance segmentation with explainability is both feasible and clinically valuable. PolypSeg-GradCAM not only achieves state-of-the-art accuracy but also bridges the critical trust gap between AI-driven predictions and real-world medical decision-making. By addressing both performance and interpretability, the proposed framework lays a foundation for future AI systems that are not only accurate but also transparent, reliable, and aligned with the needs of clinical practice.

### **Acknowledgements**

The authors would like to thank the creators and maintainers of the **Kvasir-SEG dataset** for providing an open-access benchmark that has enabled significant progress in gastrointestinal image analysis research. We also acknowledge the support of colleagues and collaborators whose insights and feedback contributed to the development of this work.

### **Data Availability**

The dataset employed in this study, **Kvasir-SEG**, is publicly available and open access. It can be freely accessed by the research community through the dataset's official publication [27] and associated hosting platform: <https://datasets.simula.no/kvasir-seg>.

### **Ethical Statement**

All images used in this study were de-identified prior to release, in compliance with ethical and privacy regulations. Since the Kvasir-SEG dataset is publicly available and anonymized, no additional institutional ethical approval was required. This research was conducted in accordance with established ethical guidelines for medical imaging research and data protection standards.

### **Conflict of Interest**

The authors declare that there are no conflicts of interest related to the publication of this work.

### **Funding**

This research did not receive external funding. The work was carried out using institutional resources and computational facilities available to the authors.

### **References**

1. Singh A. Global burden of five major types of gastrointestinal cancer. *Gastroenterology Review*. 2024;19(3):236–54.
2. Liang Y, Zhang N, Wang M, Liu Y, Ma L, Wang Q, et al. Distributions and Trends of the Global Burden of Colorectal Cancer Attributable to Dietary Risk Factors over the Past 30 Years. *Nutrients*. 2023 Dec 30;16(1):132.
3. WHO. Colorectal cancer [Internet]. World Health Organization (WHO). 2023 [cited 2025 Sep 2]. Available from: <https://www.who.int/news-room/fact-sheets/detail/colorectal-cancer>

4. Alzahrani S, Al Doghaither H, Al-Ghafari A. General insight into cancer: An overview of colorectal cancer (Review). *Mol Clin Oncol*. 2021 Nov 1;15(6):271.
5. Pinheiro M, Moreira DN, Ghidini M. Colon and rectal cancer: An emergent public health problem. *World J Gastroenterol*. 2024 Feb 21;30(7):644–51.
6. Li Y, Piao Z, Ge X, Feng J, Sun D, Zhang J. Environmental pollutants and rectal cancer: The impact of water contamination. *Ecotoxicol Environ Saf*. 2025 Apr;294:118072.
7. Kuo E, Wang K, Liu X. A Focused Review on Advances in Risk Stratification of Malignant Polyps. *Gastroenterology Res*. 2020;13(5):163–83.
8. Aarons CB, Shanmugan S, Bleier JI. Management of malignant colon polyps: Current status and controversies. *World J Gastroenterol*. 2014;20(43):16178.
9. Shussman N, Wexner SD. Colorectal polyps and polyposis syndromes. *Gastroenterol Rep (Oxf)*. 2014 Feb 1;2(1):1–15.
10. Luo Y, Zhang Y, Liu M, Lai Y, Liu P, Wang Z, et al. Artificial Intelligence-Assisted Colonoscopy for Detection of Colon Polyps: a Prospective, Randomized Cohort Study. *Journal of Gastrointestinal Surgery*. 2021 Aug;25(8):2011–8.
11. Lee A, Tutticci N. Enhancing polyp detection: technological advances in colonoscopy imaging. *Transl Gastroenterol Hepatol*. 2021 Oct;6:61–61.
12. Qayoom A, Xie J, Ali H. Polyp segmentation in medical imaging: challenges, approaches and future directions. *Artif Intell Rev*. 2025 Mar 17;58(6):169.
13. Jha D, Ali S, Tomar NK, Johansen HD, Johansen D, Rittscher J, et al. Real-Time Polyp Detection, Localization and Segmentation in Colonoscopy Using Deep Learning. *IEEE Access*. 2021;9:40496–510.
14. Asare A, Sagoe M, Asare JW. FUTransUNet-GradCAM: A Hybrid Transformer-U-Net with Self-Attention and Explainable Visualizations for Foot Ulcer Segmentation. In 2025. Available from: <https://api.semanticscholar.org/CorpusID:280537057>
15. Asare A, Gookyi DAN, Boateng D, Wulnye FA. Deploying and Evaluating Multiple Deep Learning Models on Edge Devices for Diabetic Retinopathy Detection. 2025 Jun 14;
16. Asare A, Adjei Broni A, Asare Dickson AK, Sagoe M, Cudjoe JM. Performance of ResNet-18 and InceptionResNetV2 in Automated Detection of Diabetic Retinopathy. *Medicine Advances*. 2025 Jul 15;
17. Yan T, Qin YY, Wong PK, Ren H, Wong CH, Yao L, et al. Semantic Segmentation of Gastric Polyps in Endoscopic Images Based on Convolutional Neural Networks and an Integrated Evaluation Approach. *Bioengineering*. 2023 Jul 5;10(7):806.
18. Yao W, Bai J, Liao W, Chen Y, Liu M, Xie Y. From CNN to Transformer: A Review of Medical Image Segmentation Models. *Journal of Imaging Informatics in Medicine*. 2024 Mar 4;37(4):1529–47.
19. Wu H, Zhao Z, Wang Z. META-Unet: Multi-Scale Efficient Transformer Attention Unet for Fast and High-Accuracy Polyp Segmentation. *IEEE Transactions on Automation Science and Engineering*. 2024 Jul;21(3):4117–28.
20. Wang J, Ruhaiyem NIR, Fu P. A Comprehensive Review of U-Net and Its Variants: Advances and Applications in Medical Image Segmentation. *ArXiv [Internet]*. 2025;abs/2502.06895. Available from: <https://api.semanticscholar.org/CorpusID:276259282>

21. Cao H, Wang Y, Chen J, Jiang D, Zhang X, Tian Q, et al. Swin-Unet: Unet-Like Pure Transformer for Medical Image Segmentation. In 2023. p. 205–18.
22. Chen J, Mei J, Li X, Lu Y, Yu Q, Wei Q, et al. TransUNet: Rethinking the U-Net architecture design for medical image segmentation through the lens of transformers. *Med Image Anal.* 2024 Oct;97:103280.
23. Pachetti E, Colantonio S. A systematic review of few-shot learning in medical imaging. *Artif Intell Med.* 2024 Oct;156:102949.
24. Selvaraju RR, Cogswell M, Das A, Vedantam R, Parikh D, Batra D. Grad-CAM: Visual Explanations from Deep Networks via Gradient-based Localization. 2016 Oct 7;
25. de Vries BM, Zwezerijnen GJC, Burchell GL, van Velden FHP, Menke-van der Houven van Oordt CW, Boellaard R. Explainable artificial intelligence (XAI) in radiology and nuclear medicine: a literature review. *Front Med (Lausanne).* 2023 May 12;10.
26. Muhammad D, Bendeche M. Unveiling the black box: A systematic review of Explainable Artificial Intelligence in medical image analysis. *Comput Struct Biotechnol J.* 2024 Dec;24:542–60.
27. Jha D, Smedsrud PH, Riegler MA, Halvorsen P, de Lange T, Johansen D, et al. Kvasir-SEG: A Segmented Polyp Dataset. In 2020. p. 451–62.
28. Zhang K, Wang H, Cheng Y, Liu H, Gong Q, Zeng Q, et al. Early gastric cancer detection and lesion segmentation based on deep learning and gastroscopic images. *Sci Rep.* 2024 Apr 3;14(1):7847.
29. Li H, Zhang D, Yao J, Han L, Li Z, Han J. ASPS: Augmented Segment Anything Model for Polyp Segmentation. 2024 Jun 30; Available from: <http://arxiv.org/abs/2407.00718>
30. Jha D, Ali S, Emanuelsen K, Hicks SA, Thambawita V, Garcia-Ceja E, et al. Kvasir-Instrument: Diagnostic and Therapeutic Tool Segmentation Dataset in Gastrointestinal Endoscopy. In 2021. p. 218–29.
31. Chandrakantha T S, Basavaraj N Jagadale. Comparative Analysis of U-Net and DeepLab for Automatic Polyp Segmentation in Colonoscopic Frames Using CVC-ClinicDB Dataset. *Int J Sci Res Sci Technol.* 2023 Oct 10;612–8.
32. Jha D, Sharma V, Banik D, Bhattacharya D, Roy K, Hicks SA, et al. Validating polyp and instrument segmentation methods in colonoscopy through Medico 2020 and MedAI 2021 Challenges. *Med Image Anal.* 2025 Jan;99:103307.
33. Goceri E. Polyp Segmentation Using a Hybrid Vision Transformer and a Hybrid Loss Function. *Journal of Imaging Informatics in Medicine.* 2024 Jan 12;37(2):851–63.
34. Tesema FB, Manzanares AG, Cui T, Zhang Q, Solomon M, He S. LGPS: A Lightweight GAN-Based Approach for Polyp Segmentation in Colonoscopy Images. 2025 Mar 24; Available from: <http://arxiv.org/abs/2503.18294>
35. Islam R, Akash RS, Hossen Rony MA, Hasan MZ. SAMU-Net: A dual-stage polyp segmentation network with a custom attention-based U-Net and segment anything model for enhanced mask prediction. *Array.* 2024 Dec;24:100370.
36. Yeung M, Sala E, Schönlieb CB, Rundo L. Unified Focal loss: Generalising Dice and cross entropy-based losses to handle class imbalanced medical image segmentation. *Computerized Medical Imaging and Graphics.* 2022 Jan;95:102026.

37. Koishiyeva D, Kang JW, Iliev T, Bissembayev A, Mukasheva A. Analysis of Loss Functions for Colorectal Polyp Segmentation Under Class Imbalance. In: EEPES 2025. Basel Switzerland: MDPI; 2025. p. 17.
38. Hussein BM, Shareef SM. An Empirical Study on the Correlation between Early Stopping Patience and Epochs in Deep Learning. ITM Web of Conferences. 2024 Jul 5;64:01003.